JACS
JOURNAL OF THE AMERICAN CHEMICAL SOCIETY
Cite This: J. Am. Chem. Soc. 2019, 141, 13739−13743
Communication
pubs.acs.org/JACS

Ground State Destabilization in Uracil DNA Glycosylase: Let's Not Forget "Tautomeric Strain" in Substrates

Ranjita Das,[†] Erik A. Vázquez-Montelongo,[‡] G. Andrés Cisneros,[‡] and Judy I. Wu*[,†]

[†]Department of Chemistry, University of Houston, Houston, Texas 77204, United States
[‡]Department of Chemistry, University of North Texas, Denton, Texas 76201, United States

Supporting Information

ABSTRACT: Enzymes like uracil DNA glycosylase (UDG) can achieve ground state destabilization, by polarizing substrates to mimic rare tautomers. On the basis of computed nucleus independent chemical shifts, NICS(1)$_{zz}$, and harmonic oscillator model of electron delocalization (HOMED) analyses, of quantum mechanics (QM) and quantum mechanics/molecular mechanics (QM/MM) models of the UDG active site, uracil is strongly polarized when bound to UDG and resembles a tautomer >12 kcal/mol higher in energy. Natural resonance theory (NRT) analyses identified a dominant O2 imidate resonance form for residue bound 1-methyl-uracil. This "tautomeric strain" raises the energy of uracil, making uracilate a better than expected leaving group. Computed gas-phase S_N2 reactions of free and hydrogen bonded 1-methyl-uracil demonstrate the relationship between the degree of polarization in uracil and the leaving group ability of uracilate.

In this Communication, we present computational evidence showing that enzyme environments can polarize substrates to mimic rare tautomers and, in this way, achieve ground state destabilization[1,2] through substrate strain. In the active site of uracil DNA glycosylase (UDG), uracil is polarized, and the resulting structure bears resemblance to a tautomeric form that is much higher in energy.

UDG is a base excision repair enzyme that removes mutagenic uracil from DNA by cleaving the glycosidic N1−C1′ bond of uridine. Among the family of base excision repair enzymes, UDG is the most efficient and well-characterized, showing an enormous catalytic rate acceleration of 10^{12}-fold. Studies based on NMR, Raman, kinetic isotope effect measurements, and quantum mechanics/molecular mechanics (QM/MM) computations established a stepwise dissociative mechanism, involving uracilate as the leaving group[3−17] (Figure 1a).

However, a puzzle regarding UDG is how it activates the removal of N1 deprotonated uracilate. In water (pH = 7), uracil N1—H has a pK_a of 9.8 (i.e., only as acidic as ammonium), and N1 deprotonated uracilate is not considered to be a very good leaving group at all. Parikh and Tainer et al. suggested that, in UDG, uridine adopts a strained conformation that weakens the glycosidic N1—C1′ bond through anomeric effects.[10] Drohat and Stivers showed, on the basis of NMR experiments, that uracil displayed increased acidity (pK_a = 6.4) in the active site of UDG, indicating the appearance of an O2 imidate form.[11,12] Wetmore et al. showed that uracil exhibited increased acidity when hydrogen bonded at the C=O and N—H sites.[18,19] Nevertheless, Lee et al. pointed out that increased (thermodynamic) acidity in uracil cannot be used to reason the (kinetic) leaving group ability of uracilate in UDG.[20−22] In the gas phase, uracil N1−H is as acidic as HCl, but the leaving group ability of N1 deprotonated uracilate is much poorer compared to that of Cl^-.[21]

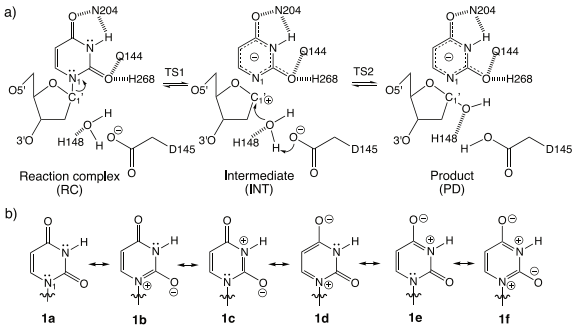

Figure 1. (a) Proposed stepwise dissociative pathway for UDG. (b) Diketo (**1a**) and imidate (**1b**−**1f**) resonance forms of uracil.

Here, we show that when uracil is bound to UDG, it does not exist in the canonical diketo form (**1**) but instead transforms to a structure akin to a rare tautomer of uracil.[23−28] In UDG, uracil forms short hydrogen bonds to several nearby residues (His268, Asn204, Gln144, and the backbone of Gln144). These hydrogen bonding interactions polarize the π-electrons of uracil, increase cyclic $[4n + 2]$ π-electron delocalization in the ring (see resonance forms **1b**−**1f**, in Figure 1b), and the resulting polarized uracil mimics a higher energy keto−enol tautomer (**2** and **3**, see also the dienol form, **4**, Figure 2). Notably, all of these tautomers are >12 kcal/mol higher in energy than the canonical diketo form (**1**) (see ΔE_T computed in the gas phase and at ε = 4, Figure 2). A dielectric constant (ε) of 4.0 was employed to simulate the enzyme active site environment.[29−31] Computed relative energies for residue−tautomer complexes are provided in the Supporting Information, SI, for comparison (see Table S1). We now show that this "tautomeric strain" raises the energy of uracil in UDG, bringing it closer to the transition state structure for N1−C1′

Received: June 17, 2019
Published: August 22, 2019

DOI: 10.1021/jacs.9b06447
J. Am. Chem. Soc. 2019, 141, 13739−13743

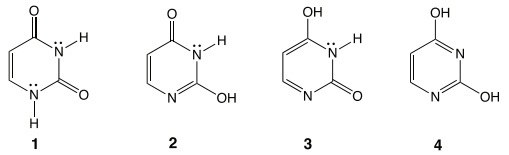

	1	2	3	4
ΔE_T (kcal/mol)	0.0 (0.0)	12.8 (14.6)	23.0 (21.1)	16.1 (19.1)
NICS(1)$_{zz}$ (ppm)	−2.5	−8.2	−7.9	−19.9
HOMED	0.701	0.774	0.800	0.994

Figure 2. Computed tautomerization energies (ΔE_T) in the gas phase and at $\varepsilon = 4$ (values in parentheses), NICS(1)$_{zz}$, and HOMED for the canonical diketo form of uracil (**1**), and its keto−enol (**2**, **3**) and dienol (**4**) tautomers.

bond cleavage. In this way, ground state destabilization helps reduce the activation barrier to expel uracilate.

According to computed nucleus independent chemical shifts,[32,33] NICS(1)$_{zz}$, uracil, **1**, is essentially nonaromatic (−2.5 ppm), and solvation in water, based on either implicit (−3.9 ppm, employing the IEF-PCM approach) or explicit (−3.3 ppm, including three water molecules) models, increases its aromaticity negligibly. This implies that solvating naked uracil in aqueous solution has a minor effect on its tautomeric form. However, when uracil is bound to the active site of UDG, it becomes markedly aromatic. NICS(1)$_{zz}$ values computed for uracil in truncated QM (−7.9 ppm) and QM/MM (−12.9 ppm) models of the UDG active site document significant aromaticity gain, suggesting a close resemblance of the electronic structure of the substrate to the rare tautomers of uracil. Despite being higher in energy, **2** (−8.2 ppm), **3** (−7.9 ppm), and **4** (−19.9 ppm) are all more aromatic than **1** (−2.5 ppm) (Figure 2). Differences in the estimated aromaticity gain of uracil based on QM and QM/MM models suggest that uracil is "aromatized" not only by nearby hydrogen bonding residues but also by other long-range electrostatic interactions in the active site of UDG. See the description of truncated QM and QM/MM models in the Computational Methods section.

Harmonic oscillator model of electron delocalization (HOMED) values,[34] a geometric index for aromaticity, indicate significant aromaticity gain for uracil **1** (0.701) when its geometry is considered in truncated QM (0.789) and QM/MM (0.829) models of the UDG active site (cf. HOMED values for **2**, 0.774; **3**, 0.800; **4**, 0.994). HOMED values close to 1 indicate fully aromatic rings. This "aromatizing" effect brings the uracil substrate closer in geometry to the N1 deprotonated uracilate (HOMED: 0.811). Natural resonance theory (NRT) analyses[35−37] for 1-methyl-uracil reveal a dominant diketo resonance form **1a** (31.3%), followed by smaller weights for the O2 imidate (16.5%) and O4 imidate (7.9%) forms. However, when 1-methyl-uracil is hydrogen bonded to His, Asn, a fragment of protein backbone, and freely optimized, the resonance weight of **1a** decreases (15.0%), while those of O2 imidate (24.1%) and O4 imidate (19.5%) increase. Changes in these resonance weights suggest that, in UDG, the electronic structure of polarized uracil resembles its keto−enol tautomers (**2** and **3**), which are 12−23 kcal/mol higher in energy. We note that the dominant O2 imidate form of hydrogen bonded 1-methyl-uracil agrees with Drohat and Stivers' finding of increased acidity of uracil due to the appearance of an O2 imidate.

Remarkably, the majority of aromaticity gain in uracil happens as soon as it is transferred from a nonenzymic environment (i.e., in water) into the UDG active site. From there, the geometry and electronic distribution of uracil already resemble a higher energy keto−enol tautomer, and the incipient uracilate is set up to be a better than expected leaving group. We computed NICS(1)$_{zz}$ for uracil and uracilate rings at stationary points along the computed reaction potential energy surface and found that uracil continues to gain aromaticity throughout the stepwise dissociative reaction: RC (−7.9 ppm), TS1 (−9.4 ppm), INT (−10.8 ppm), TS2 (−11.3 ppm), PD (−11.2 ppm) (see Figure 4). All stationary points were computed on the basis of a constrained and truncated QM model of the UDG active site, and the relative energies closely follow prior QM/MM studies.[15]

We note that "aromatization" of uracilate can also contribute to preferential enzyme−substrate binding in the transition

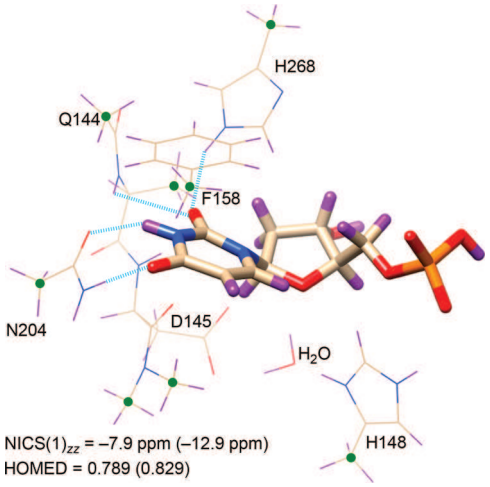

Figure 3. Truncated QM model of the UDG active site: Green dots and blue dashed lines indicate fixed positions of atoms and bond distances during geometry optimization. Computed NICS(1)$_{zz}$ and HOMED values for uracil in the truncated QM model (values based on the QM/MM model are in parentheses).

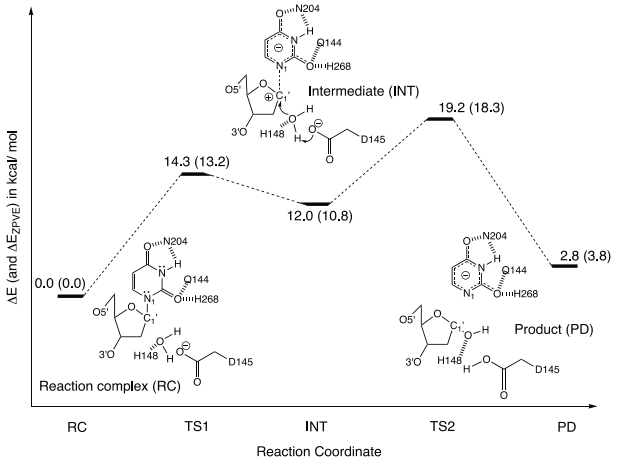

Figure 4. Relative energies (ΔE, in kcal/mol) of computed stationary points along the stepwise dissociative pathway of UDG, based on a constrained and truncated QM model (see the Computational Methods section for details) of the UDG active site. Values corrected for zero-point energy vibration (ZPVE) are shown in parentheses (ΔE_{ZPVE}, in kcal/mol). Geometries of all stationary points were optimized at ωB97X-D/6-31+G(d).

DOI: 10.1021/jacs.9b06447
J. Am. Chem. Soc. 2019, 141, 13739−13743

state. We have shown that hydrogen bonding interactions that polarize π-electrons to increase the aromatic character of heterocycles become stronger than expected.[38,39] At the transition state, hydrogen bonding interactions between the UDG active site residues and uracil polarize the π-electrons of uracil to increase aromaticity; in this way, the corresponding hydrogen bonds are strengthened, and preferential binding can happen.

As a model to probe the effect of hydrogen bonding on barrier to N−C bond cleavage, we computed gas-phase S_N2 reaction barriers for free and hydrogen bonded 1-methyl-uracil (with formate as the nucleophile). In the absence of hydrogen bonding interactions, the activation free energy barrier for N−CH_3 bond cleavage is ΔG_a = 37.8 kcal/mol, but the barrier reduces when 1-methyl-uracil is hydrogen bonded to three waters (35.7 kcal/mol) and even more so when 1-methyl-uracil is hydrogen bonded to two zwitterionic glycines (33.3 kcal/mol) (see Figure S1 in the SI). Computed $NICS(1)_{zz}$ values show that these changes correlate to increased aromaticity in 1-methyl-uracil in the reaction complex (free 1-methyl-uracil, −4.0 ppm; bound to three waters, −5.0 ppm; bound to two glycines, −5.8 ppm)—increased aromaticity in 1-methyl-uracil enhances the leaving group ability of uracilate. As the uracil ring becomes structurally more like its rare keto−enol tautomers, uracilate becomes a better leaving group.

Tautomeric strain is one way to raise the energy of substrates in enzymes, and recognizing this mode of ground state destabilization has important interpretive merit for understanding how enzymes work. Although examples of electronic strain in substrates have been reported for various enzymes, for example, substrates with polarized C═O, C═C, and C—H bonds or red-shifted UV absorptions,[40] the possibility and impact of substrate tautomerization have not been fully appreciated. Other enzymes that catalyze the glycosidic hydrolysis or biosynthesis of purine or pyrimidine substrates may take advantage of a similar mechanistic trick.

Computational Methods. All quantum mechanical (QM) geometries were optimized at ωB97X-D/6-31+G(d) in the gas phase employing Gaussian09.[41] Vibrational frequency analyses verified the nature of the stationary points. Computed nucleus independent chemical shifts (NICS),[32,33] harmonic oscillator model of electron delocalization (HOMED),[34] and natural resonance theory (NRT)[35,36] data were performed at the same level. Computations in implicit solvation employed the IEF-PCM model.

A QM model of the UDG active site was computed based on a modified, constrained, and geometry optimized crystal structure of a UDG-inhibitor complex (PDBID: 1EMH). In the pdb file, the positions of atoms C1 and N5 in the deoxypseudouridine substrate were exchanged to give a deoxyuridine substrate containing a N1−C1′ glycosidic bond. Residues and protein backbone fragments that formed hydrogen bonding (His268, Asn204, Gln144, and the backbone of Gln144) and π-stacking (Phe158) interactions to uracil, along with those relevant for activating (His148 and Asp145) the nucleophilic water molecule, were included to the model and truncated at selected carbon positions. Prior QM/MM studies document the important roles of these residues in UDG.[15] The 5′ phosphate group was included because of its recognized importance for facilitating the dissociation of uracilate. The positions of selected atoms were frozen (see green dots in Figure 3) during geometry optimization of the RC, TS1, INT, TS2, and PD. Following prior QM/MM studies, bond distances for N1−C1′ were fixed to 2.04 Å (for TS1), 2.74 Å (for INT), and 2.95 Å (for TS2), and distances between C1′ and the O atom of water were fixed to 3.04 Å (for TS1), 2.85 Å (for INT), and 1.95 Å (for TS2).[15]

All QM/MM calculations were performed using the LICHEM software package,[42,43] which employs Gaussian09 for the quantum region (QM) and TINKER8[44] for the classical region (MM). The crystal structure of a UDG-inhibitor complex was not solvated for QM/MM calculations. The QM region (UDG: Gln144, Asp145, Pro146, Tyr147, His148, Phe158, Asn204, His268, deoxyuridine, and one water molecule) was calculated at ωB97X-D/6-31+G(d). The QM/MM system involved the cleavage of covalent bonds, and thus the pseudobond approach was employed.[45] Two QM/MM simulation systems (see Figures S2 and S3 in the SI) were created on the basis of the crystal structure of a UDG-inhibitor complex: one to perform the QM/MM geometry optimization (126 QM atoms + 6 pseudobonds) and the other for the QM/MM single-point calculation (154 QM atoms + 8 pseudobonds). The MM region was modeled using the AMOEBA-BIO18 force field.[46,47]

■ ASSOCIATED CONTENT

Supporting Information

The Supporting Information is available free of charge on the ACS Publications website at DOI: 10.1021/jacs.9b06447.

Details of the HOMED method, optimized Cartesian coordinates for all QM and QM/MM structures, and computed gas-phase N−CH_3 cleavage barriers for model S_N2 reactions (PDF)

■ AUTHOR INFORMATION

Corresponding Author

*jiwu@central.uh.edu

ORCID

Judy I. Wu: 0000-0003-0590-5290

Notes

The authors declare no competing financial interest.

■ ACKNOWLEDGMENTS

J.I.W. thanks the National Science Foundation (NSF) for support (CHE-1751370) and computational resources provided by the uHPC cluster managed by the University of Houston and acquired through support from the NSF (MRI-1531814). G.A.C. thanks the UNT Department of Chemistry for the use of the HPC Cluster CRUNTCh3, as well as support from the NSF (CHE-1531468) and NIH (R01GM108583). E.A.V.-M. wishes to acknowledge CONACyT for funding. We thank Dr. Chia-Hua Wu for helpful discussions.

■ REFERENCES

(1) Jencks, W. P. *Catalysis in Chemistry and Enzymology*; McGraw-Hill: New York, 1969; p 282.

(2) Menger, F. M. Analysis of ground-state and transition-state effects in enzyme catalysis. *Biochemistry* **1992**, *31*, 5368−5373.

(3) Savva, R.; McAuley-Hecht, K.; Brown, T.; Pearl, L. The structural basis of specific base-excision repair by uracil—DNA glycosylase. *Nature* **1995**, *373*, 487−493.

(4) Mol, C. D.; Arvai, A. S.; Slupphaug, G.; Kavli, B.; Alseth, I.; Krokan, H. E.; Tainer, J. A. Crystal structure of human uracil−DNA glycosylase in complex with a protein inhibitor: Protein mimicry of DNA. *Cell* **1995**, *80*, 869−878.

DOI: 10.1021/jacs.9b06447
J. Am. Chem. Soc. 2019, 141, 13739−13743

(5) Slupphaug, G.; Mol, C. D.; Kavli, B.; Arvai, A. S.; Krokan, H. E.; Tainer, J. A. A nucleotide-flipping mechanism from the structure of human uracil—DNA glycosylase bound to DNA. *Nature* **1996**, *384*, 87−92.
(6) Kimura, E.; Kitamura, H.; Koike, T.; Shiro, M. Facile and selective electrostatic stabilization of uracil N(1)− anion by a proximate protonated amine: A chemical implication for why uracil N(1) is chosen for glycosylation site. *J. Am. Chem. Soc.* **1997**, *119*, 10909−10919.
(7) Drohat, A. C.; Jagadeesh, J.; Ferguson, E.; Stivers, J. T. Role of electrophilic and general base catalysis in the mechanism of Escherichia coli uracil DNA glycosylase. *Biochemistry* **1999**, *38*, 11866−11875.
(8) Shroyer, M. J. N.; Bennett, S. E.; Putnam, C. D.; Tainer, J. A.; Mosbaugh, D. W. Mutation of an active site residue in Escherichia coli uracil DNA glycosylase: effect on DNA binding, uracil inhibition and catalysis. *Biochemistry* **1999**, *38*, 4834−4845.
(9) Drohat, A. C.; Xiao, G.; Tordova, M.; Jagadeesh, J.; Pankiewicz, K. W.; Watanabe, K. A.; Gilliland, G. L.; Stivers, J. T. Heteronuclear NMR and crystallographic studies of wild-type and H187Q Escherichia coli uracil DNA glycosylase: electrophilic catalysis of uracil expulsion by a neutral histidine 187. *Biochemistry* **1999**, *38*, 11876−11886.
(10) Parikh, S. S.; Walcher, G.; Jones, G. D.; Slupphaug, G.; Krokan, H. E.; Blackburn, G. M.; Tainer, J. A. Uracil-DNA glycosylase-DNA substrate and product structures: conformational strain promotes catalytic efficiency by coupled stereoelectronic effects. *Proc. Natl. Acad. Sci. U. S. A.* **2000**, *97*, 5083−5088.
(11) Drohat, A. C.; Stivers, J. T. Escherichia coli uracil DNA glycosylase: NMR characterization of the short hydrogen bond from His187 to uracil O2. *Biochemistry* **2000**, *39*, 11865−11875.
(12) Drohat, A. C.; Stivers, J. T. NMR evidence for an unusually low N1 pKa for uracil bound to uracil DNA glycosylase: implications for catalysis. *J. Am. Chem. Soc.* **2000**, *122*, 1840−1841.
(13) Werner, R. M.; Stivers, J. T. Kinetic isotope effect studies of the reaction catalyzed by uracil DNA glycosylase: evidence for an oxocarbenium ion−uracil anion intermediate. *Biochemistry* **2000**, *39*, 14054−14064.
(14) Dong, J.; Drohat, A. C.; Stivers, J. T.; Pankiewicz, K. W.; Carey, P. R. Raman spectroscopy of uracil DNA glycosylase-DNA complexes: insights into DNA damage recognition and catalysis. *Biochemistry* **2000**, *39*, 13241−13250.
(15) Dinner, A. R.; Blackburn, G. M.; Karplus, M. Uracil-DNA glycosylase acts by substrate autocatalysis. *Nature* **2001**, *413*, 752−755.
(16) Stivers, J. T.; Jiang, Y. L. A mechanistic perspective on the chemistry of DNA repair glycosylases. *Chem. Rev.* **2003**, *103*, 2729−2759.
(17) Parker, J. B.; Stivers, J. T. Uracil DNA glycosylase: revisiting substrate-assisted catalysis by DNA phosphate anions. *Biochemistry* **2008**, *47*, 8614−8622.
(18) Whittleton, S. R.; Hunter, K. C.; Wetmore, S. D. Effects of hydrogen bonding on the acidity of uracil derivatives. *J. Phys. Chem. A* **2004**, *108*, 7709−7718.
(19) Di Laudo, M.; Whittleton, S. R.; Wetmore, S. D. Effects of hydrogen bonding on the acidity of uracil. *J. Phys. Chem. A* **2003**, *107*, 10406−10413.
(20) Kurinovich, M. A.; Lee, J. K. The acidity of uracil from the gas phase to solution: The coalescence of the N1 and N3 sites and implications for biological glycosylation. *J. Am. Chem. Soc.* **2000**, *122*, 6258−6262.
(21) Zhachkina, A.; Lee, J. K. Uracil and thymine reactivity in the gas phase: The S_N2 reaction and implications for electron delocalization in leaving groups. *J. Am. Chem. Soc.* **2009**, *131*, 18376−18385.
(22) Chen, M.; Lee, J. K. Computational studies of the gas-phase thermochemical properties of modified nucleobases. *J. Org. Chem.* **2014**, *79*, 11295−11300.
(23) Daniels, M. Tautomerism of uracil and thymine in aqueous solution: spectroscopic evidence. *Proc. Natl. Acad. Sci. U. S. A.* **1972**, *69*, 2488−2491.
(24) Tsuchiya, Y.; Tamura, T.; Fujii, M.; Ito, M. Keto-enol tautomer of uracil and thymine. *J. Phys. Chem.* **1988**, *92*, 1760−1765.
(25) Rejnek, J.; Hanus, M.; Kabelac, M.; Ryjacek, F.; Hobza, P. Correlated ab initio study of nucleic acid bases and their tautomers in the gas phase, in a microhydrated environment and in aqueous solution. Part 4. Uracil and thymine. *Phys. Chem. Chem. Phys.* **2005**, *7*, 2006−2017.
(26) Kryachko, E. S.; Nguyen, M. T.; Zeegers-Huyskens, T. Theoretical study of tautomeric forms of uracil. 1. Relative order of stabilities and their relation to proton affinities and deprotonation enthalpies. *J. Phys. Chem. A* **2001**, *105*, 1288−1295.
(27) Kurinovich, M. A.; Lee, J. K. The acidity of uracil and uracil analogs in the gas phase: four surprisingly acidic sites and biological implications. *J. Am. Soc. Mass Spectrom.* **2002**, *13*, 985−995.
(28) Colasurdo, D. D.; Pila, M. N.; Iglesias, D. A.; Laurella, S. L.; Ruiz, D. L. Tautomerism of urail and related compounds: A mass spectrum study. *Eur. J. Mass Spectrom.* **2018**, *24*, 214−224.
(29) DeYonker, N. J.; Webster, C. E. A theoretical study of phosphoryl transfers of Tyrosyl-DNA Phosphodiesterase I (Tdp1) and the possibility of a "Dead-End" phosphohistidine intermediate. *Biochemistry* **2015**, *54*, 4236−4247.
(30) Blomberg, M. R. A.; Borowski, T.; Himo, F.; Liao, R.-Z.; Siegbahn, P. E. M. Quantum chemical studies of mechanisms for metalloenzymes. *Chem. Rev.* **2014**, *114* (7), 3601−3658.
(31) Himo, F. Recent trends in quantum chemical modeling of enzymatic reactions. *J. Am. Chem. Soc.* **2017**, *139*, 6780−6786.
(32) Schleyer, P. v. R.; Maerker, C.; Dransfeld, A.; Jiao, H.; Hommes, N. J. R. v. E. Nucleus-independent chemical shifts: A simple and efficient aromaticity probe. *J. Am. Chem. Soc.* **1996**, *118*, 6317−6318.
(33) Chen, Z.; Wannere, C. S.; Corminboeuf, C.; Puchta, R.; Schleyer, P. v. R. Nucleus-independent chemical shifts (NICS) as an aromaticity criterion. *Chem. Rev.* **2005**, *105*, 3842−3888.
(34) Raczyñska, E. D.; Hallman, M.; Kolczyñska, K.; Stêpniewski, T. M. On the harmonic oscillator model of electron delocalization (HOMED) index and its application to heteroatomic π-electron systems. *Symmetry* **2010**, *2*, 1485−1509.
(35) Glendening, E. D.; Badenhoop, J. K.; Reed, A. E.; Carpenter, J. E.; Bohmann, J. A.; Morales, C. M.; Karafiloglou, P.; Landis, C. R.; Weinhold, F. *NBO*, 7.0. Theoretical Chemistry Institute, University of Wisconsin: Madison, 2018.
(36) Glendening, E. D.; Badenhoop, J. K.; Weinhold, F. Natural resonance theory: III. chemical applications. *J. Comput. Chem.* **1998**, *19*, 628−646.
(37) Glendening, E. D.; Landis, C. R.; Weinhold, F. Resonance theory reboot. *J. Am. Chem. Soc.* **2019**, *141*, 4156−4166.
(38) Wu, J. I.; Jackson, J. E.; Schleyer, P. v. R. Reciprocal hydrogen bonding-aromaticity relationships. *J. Am. Chem. Soc.* **2014**, *136*, 13526−13529.
(39) Kakeshpour, T.; Wu, J. I.; Jackson, J. E. AMHB: (anti-)aromaticity-modulated hydrogen bonding. *J. Am. Chem. Soc.* **2016**, *138*, 3427−3432.
(40) Anderson, V. E. Ground state destabilization. In *Encyclopedia of Life Sciences*; John Wiley & Sons, Ltd., 2001; www.els.net, and references therein.
(41) Frisch, M. J.; Trucks, G. W.; Schlegel, H. B.; Scuseria, G. E.; Robb, M. A.; Cheeseman, J. R.; Scalmani, G.; Barone, V.; Mennucci, B.; Petersson, G. A.; Nakatsuji, H.; Caricato, M.; Li, X.; Hratchian, H. P.; Izmaylov, A. F.; Bloino, J.; Zheng, G.; Sonnenberg, J. L.; Hada, M.; Ehara, M.; Toyota, K.; Fukuda, R.; Hasegawa, J.; Ishida, M.; Nakajima, T.; Honda, Y.; Kitao, O.; Nakai, H.; Vreven, T.; Montgomery, J. A., Jr.; Peralta, J. E.; Ogliaro, F.; Bearpark, M.; Heyd, J. J.; Brothers, E.; Kudin, K. N.; Staroverov, V. N.; Kobayashi, R.; Normand, J.; Raghavachari, K.; Rendell, A.; Burant, J. C.; Iyengar, S. S.; Tomasi, J.; Cossi, M.; Rega, N.; Millam, J. M.; Klene, M.; Knox, J. E.; Cross, J. B.; Bakken, V.; Adamo, C.; Jaramillo, J.; Gomperts, R.;

DOI: 10.1021/jacs.9b06447
J. Am. Chem. Soc. 2019, 141, 13739−13743

Stratmann, R. E.; Yazyev, O.; Austin, A. J.; Cammi, R.; Pomelli, C.; Ochterski, J. W.; Martin, R. L.; Morokuma, K.; Zakrzewski, V. G.; Voth, G. A.; Salvador, P.; Dannenberg, J. J.; Dapprich, S.; Daniels, A. D.; Farkas, O.; Foresman, J. B.; Ortiz, J. V.; Cioslowski, J.; Fox, D. J. *Gaussian 09*, revision D.01; Gaussian, Inc.: Wallingford, CT, 2009.

(42) Kratz, E. G.; Walker, A. R.; Lagardère, L.; Lipparini, F.; Piquemal, J.-P.; Andrés Cisneros, G. LICHEM: A QM/MM program for simulations with multipolar and polarizable force fields. *J. Comput. Chem.* **2016**, *37*, 1019−1029.

(43) Gökcan, H.; Vázquez-Montelongo, E. A.; Cisneros, G. A. LICHEM 1.1: recent improvements and new capabilities. *J. Chem. Theory Comput.* **2019**, *15*, 3056−3065.

(44) Rackers, J. A.; Wang, Z.; Lu, C.; Laury, M. L.; Lagardère, L.; Schnieders, M. J.; Piquemal, J.-P.; Ren, P.; Ponder, J. W. Tinker 8: Software Tools for Molecular Design. *J. Chem. Theory Comput.* **2018**, *14*, 5273−5289.

(45) Parks, J. M.; Hu, H.; Cohen, A. J.; Yang, W. A pseudobond parametrization for improved electrostatics in quantum mechanical/molecular mechanical simulations of enzymes. *J. Chem. Phys.* **2008**, *129*, 154106.

(46) Shi, Y.; Xia, Z.; Zhang, J.; Best, R.; Ponder, J. W.; Ren, P. Polarizable Atomic Multipole-Based AMOEBA Force Field for Proteins. *J. Chem. Theory Comput.* **2013**, *9*, 4046−4063.

(47) Zhang, C.; Lu, C.; Jing, Z.; Wu, C.; Piquemal, J.-P.; Ponder, J. W.; Ren, P. AMOEBA Polarizable Atomic Multipole Force Field for Nucleic Acids. *J. Chem. Theory Comput.* **2018**, *14*, 2084−2108.

DOI: 10.1021/jacs.9b06447
J. Am. Chem. Soc. 2019, 141, 13739−13743